Powder Technology 466 (2025) 121452

Contents lists available at ScienceDirect

Powder Technology

journal homepage: www.journals.elsevier.com/powder-technology

Role of particle morphology in monotonic and cyclic behavior of granular materials: Insights from cereals

Kaifeng Zeng [a,b], Zhen-Yu Yin [a,b,*], Ruidong Li [a,b], Yin-Fu Jin [c,d]

[a] Department of Civil and Environmental Engineering, The Hong Kong Polytechnic University, Hung Hom, Kowloon, Hong Kong
[b] Research Centre for Nature-based Urban Infrastructure Solutions, The Hong Kong Polytechnic University, Hong Kong
[c] State Key Laboratory of Intelligent Geotechnics and Tunnelling, Shenzhen University, Shenzhen 518060, Guangdong, China
[d] College of Civil and Transportation Engineering, Shenzhen University, Shenzhen 518060, Guangdong, China

HIGHLIGHTS

- Three-dimensional particle shapes were obtained by X-ray microcomputed tomography.
- Particle shape effect on static/cyclic behavior of granular materials was studied.
- Effect of roughness on static/cyclic behavior of granular materials was studied.
- Special mechanical behavior of the cereals with surface-adhered starch were studied.

GRAPHICAL ABSTRACT

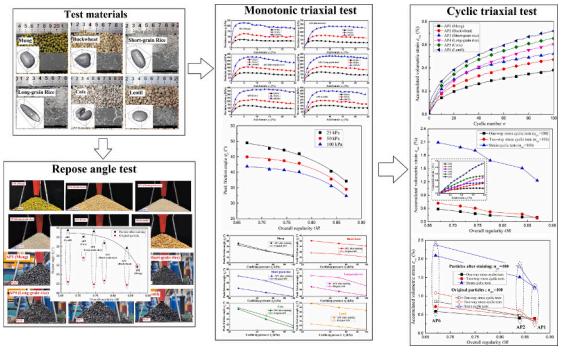

ARTICLE INFO

Keywords:
Granular material
Particle shape
Surface characteristics
triaxial test
Cyclic behavior
Friction angle
Accumulated volumetric strain

ABSTRACT

Particle morphology, as intrinsic properties of granular materials, significantly affects the mechanical response of granular materials, but little attention has been paid to cyclic response together with monotonic behavior. In this study, six cereals with similar grain sizes but different shapes were selected as testing materials due to their minimal variation in particle morphology. First, three-dimensional particle shapes of six cereals were obtained using X-ray microcomputed tomography (μCT). Then, a series of monotonic and cyclic triaxial tests were conducted on all cereals with and without staining. The staining could effectively eliminate the surface characteristic differences among six cereals, enabling them to be employed to better investigate particle shape effects. Meanwhile, since the surface characteristics of cereals, such as surface roughness and surface-adhered starch, underwent significant changes after staining, their effects could also be analyzed by comparing the results of cereals before and after staining. Repose angle tests were conducted to investigate changes in the surface roughness of six cereals after staining, which showed that staining had no significant effect on the surface roughness of mung but significantly increased it for all other cereals. Triaxial test results showed that the peak friction angle decreased with increasing particle shape regularity and decreasing surface roughness, while accumulated volumetric strain during cyclic tests decreased under both conditions. Furthermore, the cereals with surface-adhered starch exhibited quite different mechanical behavior than conventional granular materials. The

* Corresponding author at: Department of Civil and Environmental Engineering, The Hong Kong Polytechnic University, Hung Hom, Kowloon, Hong Kong.
E-mail address: zhenyu.yin@polyu.edu.hk (Z.-Y. Yin).

https://doi.org/10.1016/j.powtec.2025.121452
Received 18 May 2025; Received in revised form 30 June 2025; Accepted 21 July 2025
Available online 23 July 2025

starch bond under confining pressure significantly enhanced their shear strength and reduced their compressibility. However, the specimens experienced an abrupt strength reduction and volume contraction when the deviatoric stress reached the critical threshold of starch bond rupture, which required special attention during the storage and transportation of cereals.

Notations

C	convexity
D_e	equivalent diameter
D_{Fmax}, D_{Fmed}, D_{Fmin}	maximum, medium and minimum Feret diameters
D_r	relative density
EI, FI	elongation and flatness indices
G_s	specific gravity
k	average slope of single-particle compression curves
n_{cyc}	cyclic number
OR	overall regularity
p	mean principal stress
q	deviatoric stress
q_f	peak deviatoric stress
R	roundness
S	sphericity
ε_1	axial strain
ε_v	volumetric strain
ε_{vac}	accumulated volumetric strain
η	stress ratio
θ_r	angle of repose
ρ_{min}, $\rho_{\max}$	minimum and maximum dry densities
σ_1, σ_3	major and minor principal stresses
φ_{cs}	critical state friction angle
φ_p	peak friction angle
ψ_{max}	maximum dilatancy angle

1. Introduction

Granular materials are prevalent in nature and daily life, with applications spanning agriculture, geotechnical, pharmaceuticals, and catalysis engineering [1,2]. Granular materials act as discrete media, with their mechanical behavior arising from interactions between individual particles. Therefore, the characteristics of individual particles, such as particle size, shape and surface roughness, have a critical effect on the macroscopic mechanical behavior of granular materials [3,4]. Granular materials with different particle size distributions can be easily obtained using sieve analysis, and its effects have been extensively studied.

It is relatively difficult to study the effect of particle shape and surface roughness on the mechanical behavior of granular materials by the experimental approach. A common experimental approach to study the effect of particle shape involves preparing samples by mixing the round and angular granular materials, and the specimens with different particle shape can be obtain by changing the content of the round and angular particles [5–10]. For example, Shinohara and Golman [11] conducted a series of triaxial compression tests on the angular stainless-steel powders to investigate the effect of particle shape on the internal friction angle of fine powders, and found that the internal friction angle increased with increasing particle angularity and decreasing initial void ratio. Altuhafi et al. [12] compiled a database of the mechanical behavior of 25 natural sands, and found that the soils with lower aspect ratio had a higher critical state friction angle and the critical state friction angle became lower for more spherical particles. Xiao et al. [13] carried out a series of drained triaxial compression tests on sands mixed with angular and rounded glass beads of different proportions. The results showed that the peak friction angle decreased with increasing overall regularity, and the slope of the relationship between the peak friction angle and maximum dilatancy angle was independent of the particle shape. The sandblasting or milling techniques were usually used to obtain the particles with different surface roughness, and the effect of surface roughness on the mechanical behavior of granular materials can be analyzed by comparing their test results [14–17]. Li et al. [18] carried out the triaxial compression tests on six types of granular materials with different particle shapes and manually adjusted surface textures. The test results showed that the shear strength increased with increasing surface roughness, which is more significant in irregular particle materials. Miao et al. [19] obtained the spherical glass beads with different surface roughness using sandblasting technology and performed a series of triaxial consolidation-drained tests on them. They found that as particle surface roughness increased, the peak deviatoric stress significantly raised and the softening behavior of the stress-strain curves was more obvious. However, the particle shape or surface roughness of granular materials in previous experimental studies are usually within a certain range rather than a definite value, and the effects of particle shape or surface roughness distributions on test result analysis are difficult to eliminate. Furthermore, the two-dimensional shape parameters were used in most experimental studies due to the difficulty of capturing the three-dimensional particle shape of granular materials, which somewhat affects the reliability of the conclusions.

To overcome the limitations of the laboratory experiments, some researchers adopted the discrete element method (DEM) to study the effect of particle shape [20–31] and surface roughness [32,33] on the mechanical behavior of granular materials. Xu et al. [34] adopted the method combining Fourier shape descriptors and random field in 3D DEM simulation to generate complex shaped particles, and found that the dilation and shear strength of the granular materials increased with increasing irregularity and elongation. Nie et al. [35] used a multi-sphere method to model the three-dimensional irregular particles in 3D DEM simulation, and found that the shear strength generally decreased and the volumetric strain linearly and monotonically decreased with increasing roundness. Ali and Kikumoto [36] systematically investigated the effects of particle roundness and aspect ratio on the macro and micromechanical behaviors of granular materials using 2D DEM model. The simulation results showed that the shear strength monotonically increased with decreasing roundness, but the effect of aspect ratio on shear strength was non-monotonic and the shear strength reached the maximum value at about 0.7 aspect ratio. Fan et al. [37] investigated the dependence of shear behaviors of granular materials on particle multi-level morphology, and found that the peak and critical state friction angle increased with increasing angularity indices and roughness. Although some valuable findings acquired from the discrete element method (DEM), the simulation results are always less reliable than experimental results.

The cereals may be suitable experimental subjects to study the effect of particle shape on the mechanical behavior of granular materials. The agricultural grains with different particle shapes can be easily found in nature, and those of the same variety exhibit minimal variations in both

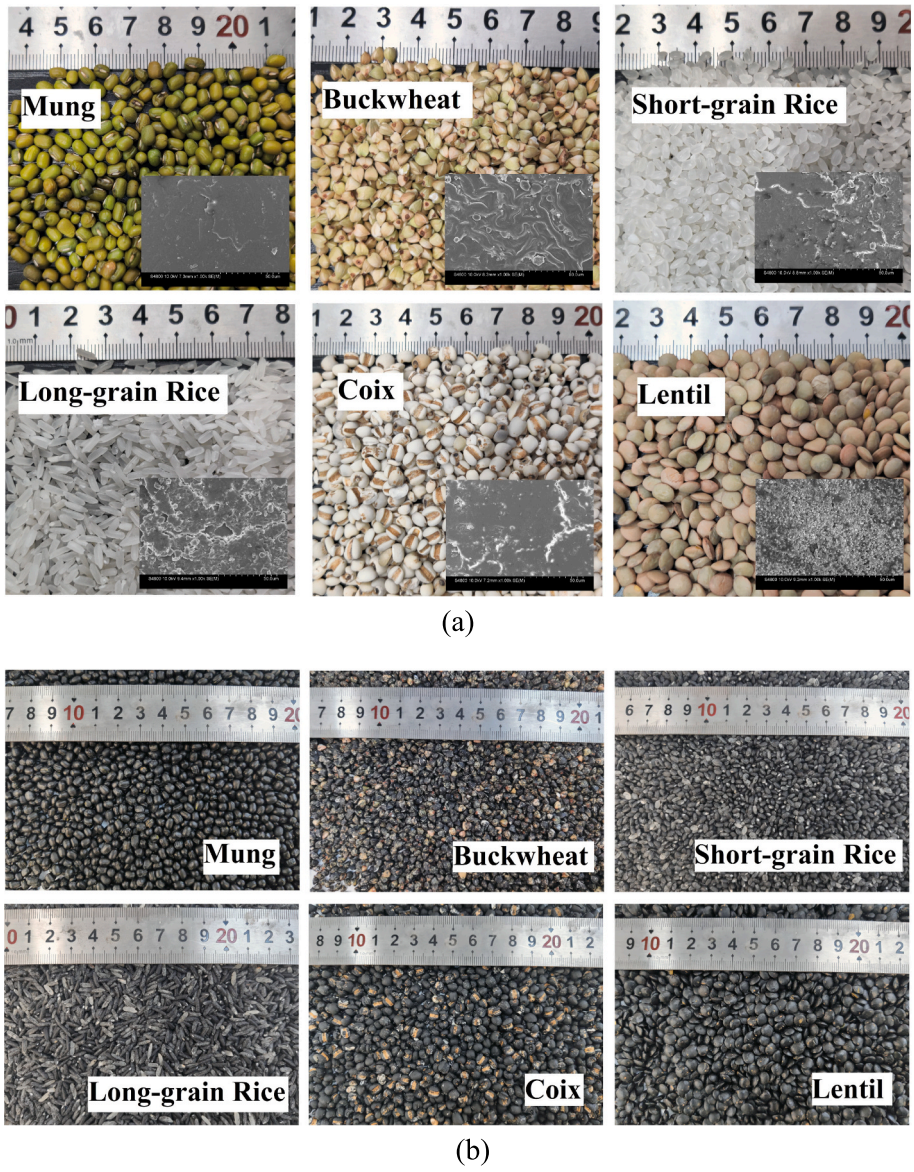

Fig. 1. Photos of cereals (a) original particles and SEM images (b) particles after staining.

size and shape. Furthermore, current research on the mechanical behavior of crop grains remains at a relatively early stage, with experiments predominantly employing direct shear tests [38–45]. Exploring the mechanical behavior of cereals under triaxial stress state is also helpful for the transportation and storage of food crops in agricultural engineering.

Therefore, six types of cereals with different particle shapes were selected as the experimental subjects in this study, and their three-dimensional particle shapes were obtained using X-ray microcomputed tomography (μCT) technology. Besides the monotonic triaxial tests, one-way stress cyclic, two-way stress cyclic, and strain cyclic triaxial tests, which have been rarely investigated, have also been conducted. The surface roughness of cereals was standardized using staining method, and the effect of particle shape were analyzed by comparing the test results of stained cereals. Furthermore, the effect of surface characteristics could be analyzed by comparing the test results of cereals before and after staining. It is hoped that the findings of this experimental program could promote the research of granular materials and shed some light on the transportation and storage of food crops in agricultural engineering.

2. Testing program

2.1. Test materials and apparatus

To investigate the effect of particle shape on the monotonic and cyclic mechanical behavior of granular materials, six types of cereals including mung, buckwheat, short-grain rice, long-grain rice, coix and lentil were used in this study. The mung, buckwheat, short-grain rice, long-grain rice, coix and lentil were sourced from Hebei, Liaoning, Anhui, Liaoning, Hebei and Gansu Provinces in China, respectively. The mung was used as the control group, which was approximately spherical in shape. The buckwheat and coix particles had distinct edges and grooves, respectively. The particle shapes of rice and lentil were elongated and flattened, respectively. The detailed particle shape analysis is presented in the next subsection. Fig. 1(a) shows the photos of six types of cereals, as well as 1000 times SEM images of their surfaces. It can be observed that there was a significant difference in the surface characteristics of six types of cereals. Therefore, those cereals were stained using acrylic paint to standardize their surface characteristics, and the stained particles (as shown in Fig. 1(b)) were used as research objects to study the effect of particle shape on the mechanical behavior of granular

Table 1
Physical properties of six types of cereals.

Type of agricultural particle		Minimum dry density ρ_{min} (g/cm^3)	Maximum dry density ρ_{max} (g/cm^3)	Specific gravity G_s
Mung	Original	0.805	0.932	1.348
	After staining	0.749	0.785	
Buckwheat	Original	0.769	0.839	1.295
	After staining	0.686	0.807	
Short-grain rice	Original	0.946	0.995	1.450
	After staining	0.741	0.881	
Long-grain rice	Original	0.824	0.943	1.479
	After staining	0.714	0.842	
Coix	Original	0.729	0.871	1.429
	After staining	0.665	0.802	
Lentil	Original	0.864	0.898	1.410
	After staining	0.667	0.815	

materials. In addition, the effect of surface characteristics on the mechanical behavior of granular materials was also investigated by comparing the test results of original and stained particles.

The minimum and maximum dry densities (ρ_{min} and ρ_{max}) of the original and stained six types of cereals were measured according to ASTM D4253–16 [46] However, due to the high water absorption capacity of cereals, the traditional method was not suitable to measure the specific gravity (G_s) of cereals. In this study, the volume and mass of cereals (V_a and m_a) were measured using X-ray microcomputed tomography (μCT) and a balance with a resolution of 0.001 g, respectively, and the specific gravity can be determined by way of $G_s = m_a/V_a$. Finally, the physical properties of six types of cereals are shown in Table 1. It can be observed that the minimum and maximum dry densities of cereals reduced after staining. Furthermore, the specific gravity of the six cereals varied slightly. However, the relative density of the six cereal specimens remained consistent in this study, so the difference in their specific gravity will not affect the findings.

A series of single-particle compression tests were performed on six types of cereals to ensure that their stiffnesses were similar. In the single-particle compression tests, the cereal particles were placed between two rigid plates and loaded at a rate of 0.1 mm/min. Their single-particle compression curves are shown in Fig. 2. During the initial loading stage, the cereal particles exhibited approximately elastic deformation, and the slope of their compressive curve was closely related to their particle stiffness. It can be found that the average slope (k) of the compression curves for six types of cereals ranged from 280 N/mm to 415 N/mm, which indicated that the six types of cereals had similar stiffnesses and their test results were comparable.

The apparatus used in the triaxial tests was the KTL-DYNTTS dynamic triaxial apparatus (Geotop Technology Zhejiang Limited, Zhejiang, China), as shown in Fig. 3. The apparatus was composed of confining and back pressure controllers, displacement/force/water pressure sensors, loading devices, and a data acquisition system. The sensors for confining, back, and water pressure had a maximum range of 2000 kPa, with an accuracy of 0.2 kPa. The maximum axial force and

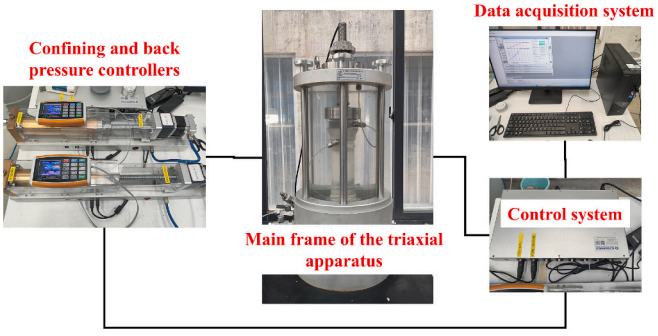

Fig. 3. Triaxial test apparatus.

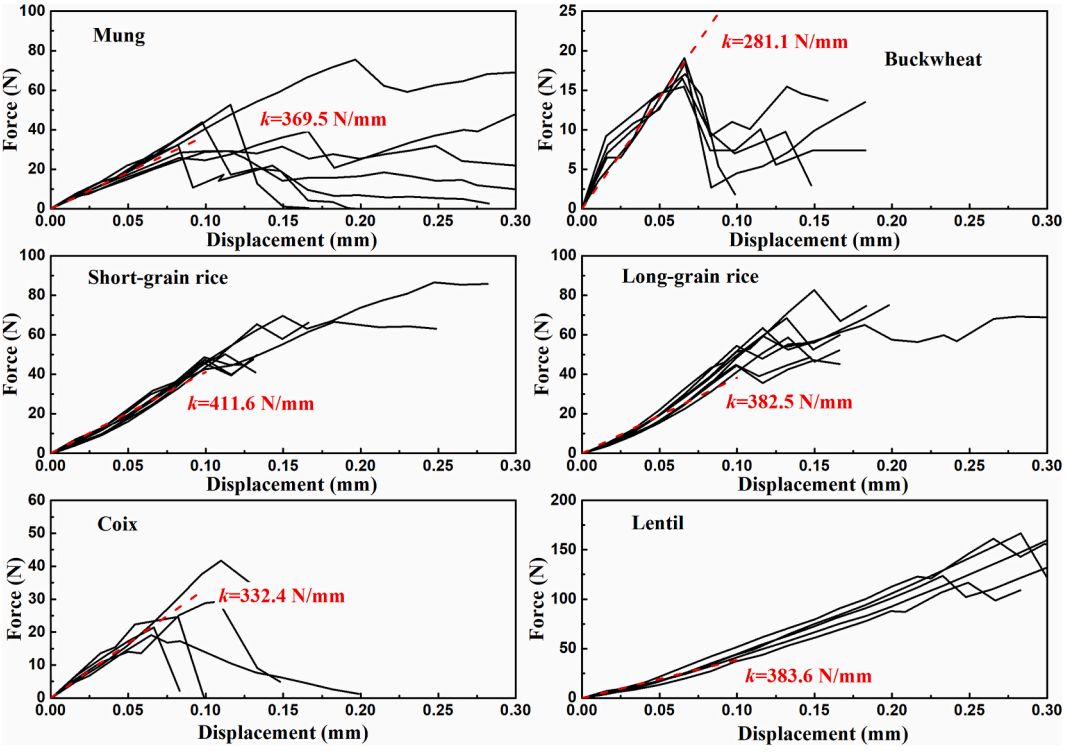

Fig. 2. Force-displacement curves of cereals in single-particle compression tests.

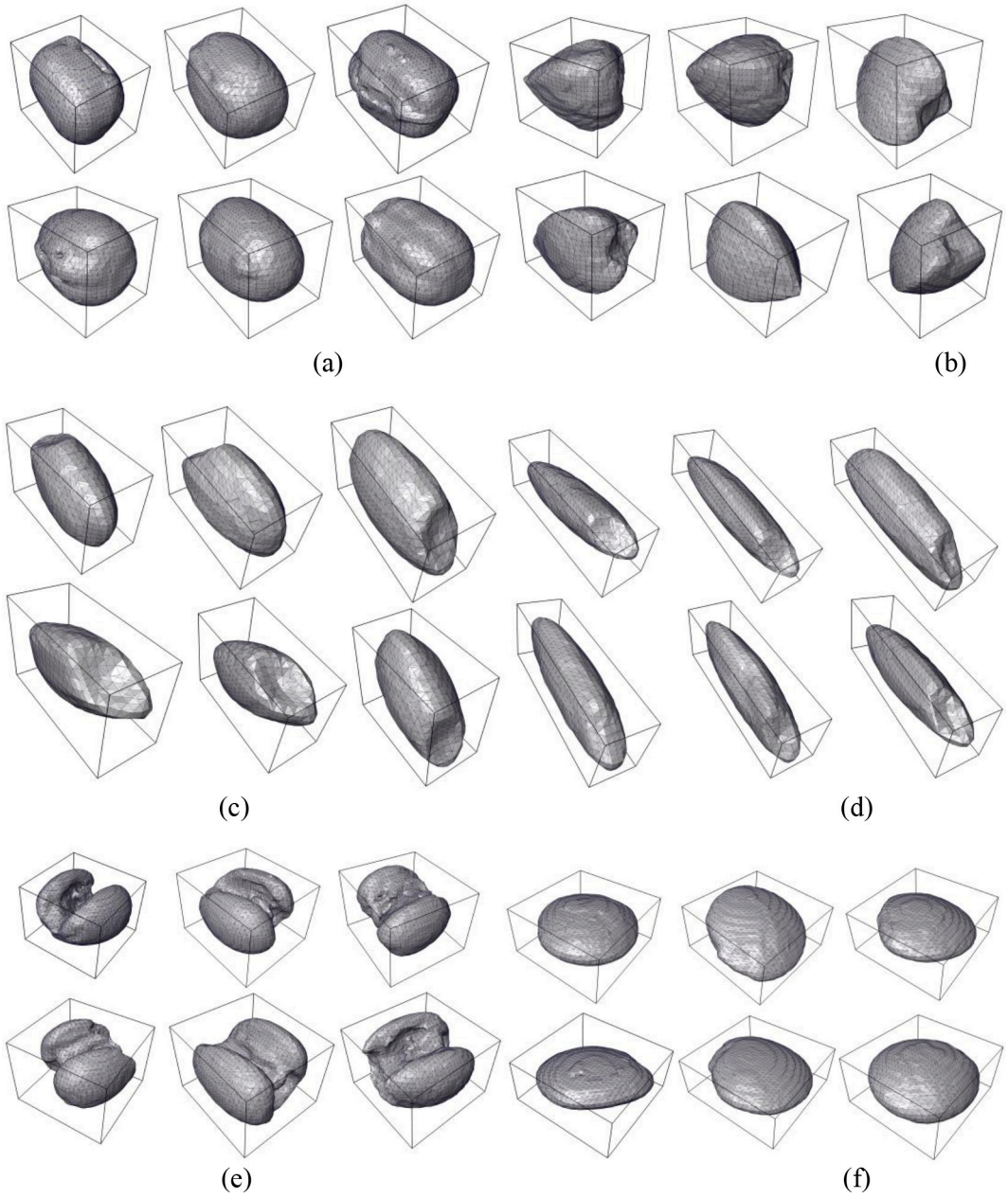

Fig. 4. 3D reconstruction of cereals (a) mung (b) buckwheat (c) short-grain rice (d) long-grain rice (e) coix (f) lentil.

displacement were 10 kN and 100 mm, with force and displacement (LVDT) sensor accuracies of 0.001 kN and 0.01 mm, respectively. The volumetric strain was measured by the water change in back or cell pressure controllers with an accuracy of 0.001 ml. All the transducers were calibrated, and the errors were within 0.1 %. In addition, the diameter and height of the specimens were 50 mm and 100 mm, respectively, and the membrane thickness was 0.3 mm.

2.2. Particle shape analysis

An X-ray microcomputed tomography (μCT) apparatus XT H 225 ST from The Hong Kong Polytechnic University, manufactured by Nikon company was employed to examine the three-dimensional particle shapes of six types of cereals. CT scanning tests with 39 μm pixels were performed on each of the six types of cereals, and more than 200 particles were tested for each agricultural particle. The particles were reconstructed using the GeoVision method proposed by Li et al. [47–49], and partial 3D reconstruction of six types of cereals is shown in Fig. 4. Their surface files in STL format can be found in the Supplemental Materials, which may be useful for the discrete element simulation of cereals. The triangular surface meshes representing cereal particles comprised approximately 5000 elements.

Four particle size parameters (i.e., maximum, medium and minimum Feret diameter D_{Fmax}, D_{Fmed} and D_{Fmin}, and equivalent diameter D_e) and five shape parameters (i.e., elongation *EI*, flatness *FI*, sphericity *S*, convexity *C* and roundness *R*) were employed to describe the three-dimensional grain characteristics of cereals. Elongation *EI* and flatness *FI* are the ratio of the medium and minimum Feret diameter to the maximum Feret diameter, respectively [50]. Sphericity *S* is the ratio of the surface area of equivalent sphere to the actual particle surface area [51]. Convexity *C* is the ratio of the actual particle volume to the volume of convex hull [51]. Roundness *R* [52] is the ratio of the average radius of corner spheres of the particle to the radius of the maximum inscribed sphere. Table 2 shows the three-dimensional particle size parameters of

Table 2
Three-dimensional particle size parameters of cereals.

Particle size parameters		Mung	Buckwheat	Short-grain rice	Long-grain rice	Coix	Lentil
Maximum Feret diameter D_{Fmax}	Mean value	5.540	4.457	4.490	6.553	5.825	5.931
	Standard deviation	0.374	0.374	0.246	0.480	0.502	0.372
	Variation coefficient	0.067	0.084	0.055	0.073	0.086	0.063
Medium Feret diameter D_{Fmed}	Mean value	4.385	3.598	2.825	2.098	5.514	5.618
	Standard deviation	0.270	0.287	0.159	0.159	0.487	0.297
	Variation coefficient	0.062	0.080	0.056	0.076	0.088	0.053
Minimum Feret diameter D_{Fmin}	Mean value	3.997	3.341	2.108	1.876	4.125	2.624
	Standard deviation	0.220	0.253	0.117	0.136	0.417	0.159
	Variation coefficient	0.055	0.076	0.056	0.072	0.101	0.061
Equivalent diameter D_e	Mean value	4.521	3.386	2.847	2.845	4.447	4.191
	Standard deviation	0.251	0.226	0.127	0.120	0.402	0.179
	Variation coefficient	0.056	0.067	0.045	0.042	0.090	0.043

Table 3
Three-dimensional particle shape parameters of cereals.

Particle shape parameters		Mung	Buckwheat	Short-grain rice	Long-grain rice	Coix	Lentil
Elongation *EI*	Mean value	0.794	0.810	0.630	0.322	0.947	0.948
	Standard deviation	0.054	0.061	0.038	0.036	0.035	0.028
	Variation coefficient	0.068	0.075	0.060	0.112	0.037	0.030
Flatness *FI*	Mean value	0.723	0.752	0.470	0.288	0.709	0.443
	Standard deviation	0.040	0.051	0.026	0.029	0.049	0.034
	Variation coefficient	0.055	0.068	0.055	0.101	0.069	0.077
Sphericity *S*	Mean value	0.915	0.874	0.867	0.720	0.654	0.812
	Standard deviation	0.041	0.044	0.012	0.026	0.084	0.019
	Variation coefficient	0.045	0.050	0.014	0.036	0.128	0.023
Convexity *C*	Mean value	0.982	0.968	0.984	0.987	0.770	0.981
	Standard deviation	0.011	0.025	0.006	0.005	0.056	0.006
	Variation coefficient	0.011	0.026	0.006	0.005	0.073	0.006
Roundness *R*	Mean value	0.815	0.673	0.807	0.833	0.696	0.648
	Standard deviation	0.061	0.051	0.033	0.023	0.037	0.031
	Variation coefficient	0.075	0.076	0.041	0.028	0.053	0.048
$OR = (FI + FI/EI + S + C + R)/5$		0.870	0.839	0.775	0.745	0.715	0.671

cereals. The equivalent diameters of six types of cereals were within the range of 2.5 mm to 5.0 mm, which indicated that the six types of cereals had similar particle size and their test results were comparable.

Table 3 shows the three-dimensional particle shape parameters of cereals, and the smaller particle shape parameters represent more irregular particle shapes. As shown in Table 3, the particle shape of mung was relatively regular. The buckwheat had a smaller roundness *R*. The short-grain and long-grain rice had smaller elongation *EI* and flatness *FI*. The coix had smaller sphericity *S* and convexity *C*. The lentil had smaller flatness *FI* and roundness *R*. Following a comprehensive comparison, the overall regularity *OR* [$= (FI + FI/EI + S + C + R)/5$] was used to characterize the comprehensive shape of cereals. The overall regularity *OR* ranges from 0 to 1, with a smaller value indicating a greater irregularity in particle shape. According to the degree of shape irregularity, the mung, buckwheat, short-grain rice, long-grain rice, coix and lentil were labeled as AP1, AP2, AP3, AP4, AP5 and AP6. Furthermore, the standard deviations and variation coefficients of all particle size and shape parameters in Table 2 and Table 3 were small, which meant that the particle size and shape distributions of cereals were pretty uniform.

2.3. Testing methods

The triaxial tests included the monotonic, one-way stress cyclic, two-way stress cyclic and strain cyclic tests of six types of cereals, both original and stained cereals. Since cereal particles soften upon contact with water, all specimens were dry and were prepared according to the standard ASTM D7181 [53]. The specimens were then consolidated under isotropic pressure until primary consolidation was finished. The subsequent tests were conducted according to the test protocols in Table 4. The exhaust valve was opened during the shearing process and the specimen volume could change. Since no pore water drainage occurred, the volumetric strain of the specimens was measured by the water volume change in confining pressure chamber. The axial strain rate of the monotonic tests was 0.2 %/min, and the frequency and the cycle number of the cyclic tests were 0.1 Hz and 100, respectively. The

Table 4
Test parameters of monotonic and cyclic triaxial tests.

Type of triaxial test	Type of agricultural particle		Relative density D_r	Confining pressure (kPa)	Cyclic deviatoric stress (kPa)		Cyclic axial strain (%)	
					Max.	Min.	Max.	Min.
Monotonic test	Original; Stained	Mung (AP1); Buckwheat (AP2); Short-grain rice (AP3); Long-grain rice (AP4); Coix (AP5); Lentil (AP6)	80 %	25; 50; 100	–	–	–	–
One-way stress cyclic test				50	60	10	–	–
Two-way stress cyclic test				50	25	−25	–	–
Strain cyclic test				50	–	–	1 %	−1 %

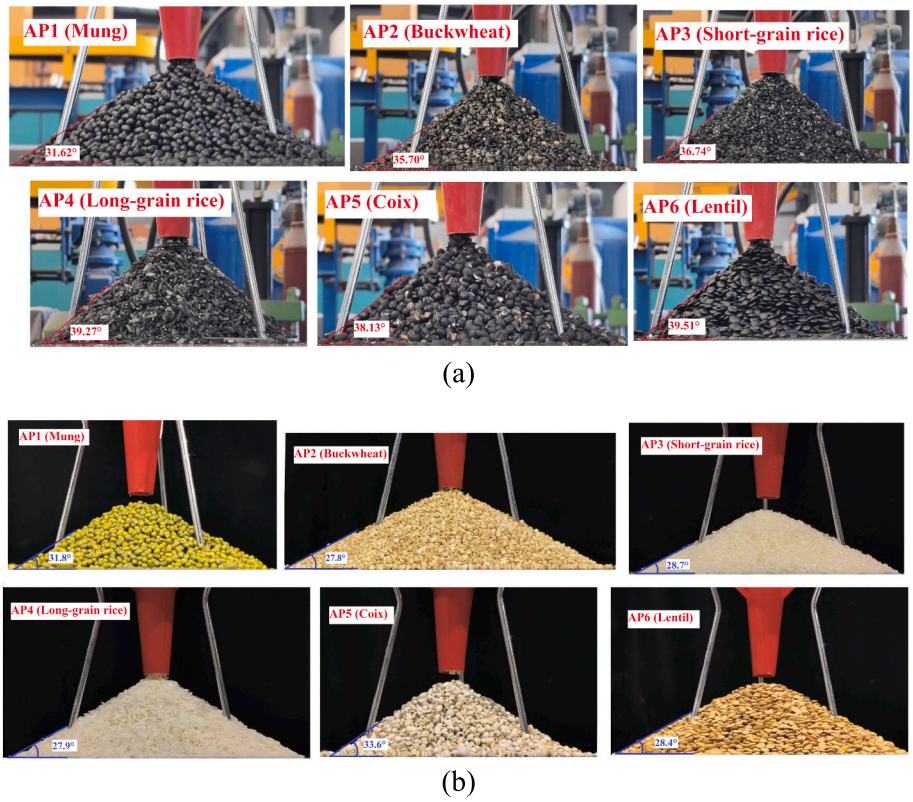

Fig. 5. Repose angles of cereals (a) particles after staining (b) original particles.

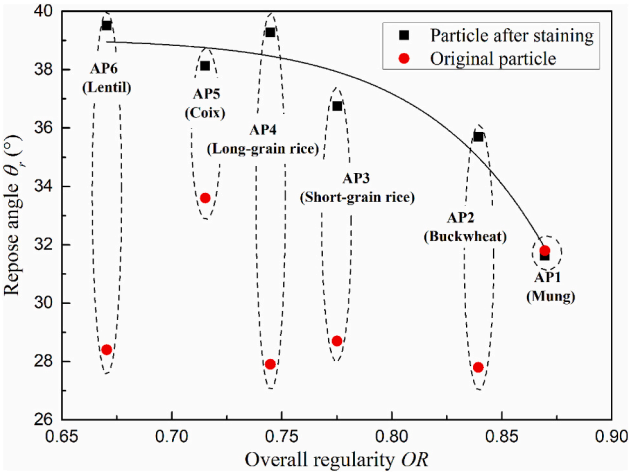

Fig. 6. Relationship between repose angle and overall regularity.

low frequency used in the cyclic tests was to avoid the boundary effect during dynamic testing [54,55]. Notably, since particle morphology influences the maximum and minimum void ratios, cereal specimens with different shapes may exhibit distinct dense states at the same void ratios. Therefore, relative density was maintained consistently in this study. In addition, the particle size distribution curves of the specimens after testing were measured through sieve analysis. The results shows that the gradation curves of all six grain specimens remained unchanged. This indicated that particle breakage can be neglected in this study.

3. Repose angle test results

Before the triaxial tests, the effect of particle shape and surface characteristics on the repose angle of cereals was investigated. The funnel method was employed to measure the angle of repose of cereal particles, with the procedure conducted as follows: First, the bottom valve of the funnel was sealed, and cereal particles were filled into the funnel. Subsequently, the bottom valve was opened to allow particles to free-fall onto the base plate. Finally, after particles completely ceased moving, the inclination angle of the formed pile was measured. The test was repeated five times to ensure result reliability, and the angle of repose of the cereal particles was taken as the mean value of the five measurements. The test results of original and stained cereals are shown in Fig. 5 and Fig. 6. As shown in Fig. 6, the repose angles of stained cereals decreased with increasing the overall regularity, which indicated that when the surface characteristics were similar, the more irregular the particle shape was, the larger the repose angle was. A comparison of repose angles of cereals before and after staining showed that staining had no significant effect on the surface roughness of mung but significantly increased it for all other cereals.

4. Monotonic mechanical behavior

4.1. Effect of particle shape

Figs. 7(a) and (b) show the monotonic deviatoric stress-volumetric strain-axial strain relationships of the stained cereals. The soft cereals exhibited similar behaviors to the hard granular materials such as sand particles. The deviatoric stress-axial strain curves hardened and then softened, and the volumetric strain- axial strain curves contracted and then dilated. As the confining pressure increased, the initial shear modulus increased, the peak deviatoric stress increased and the softening and dilatancy became less evident. Furthermore, the axial strains at the peak state and the phase transformation state (from compression

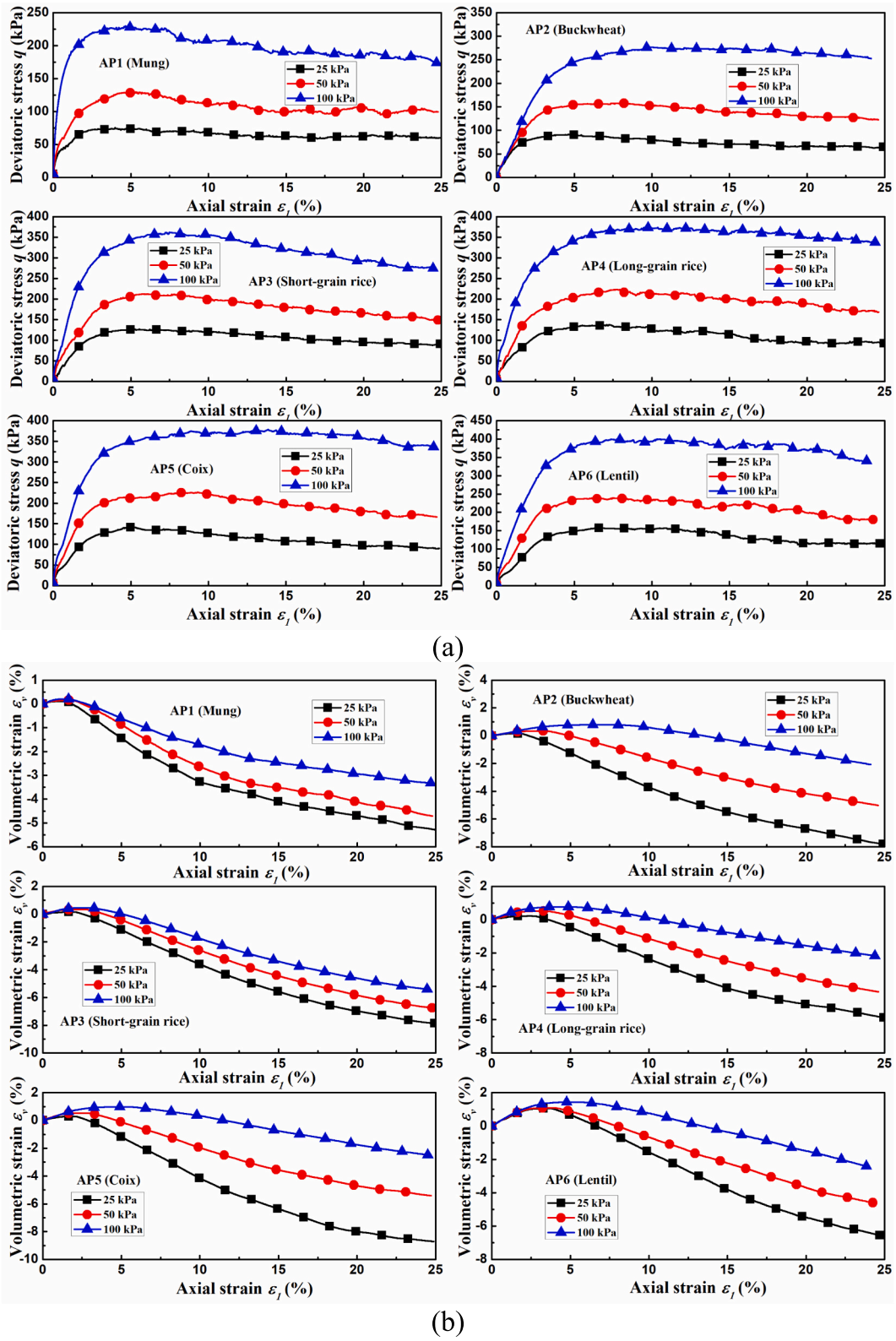

Fig. 7. Monotonic stress-strain relationships of the cereals after staining (a) deviatoric stress-axial strain relationships (b) volumetric strain-axial strain relationships.

to dilatancy) also increased with increasing confining pressure.

In addition, it can be found by comparing the results of mung particles with other cereals that the peak deviatoric stress increased with decreasing elongation index *EI*, flatness index *FI*, sphericity *S*, convexity *C* and roundness *R*. The similar phenomenon was also found in some discrete element simulations [32,33] and tests on sand particles or glass beads [12,13].

Fig. 8(a) shows the relationship between the peak friction angle φ_{max} and the overall regularity *OR* under different confining pressures. The peak friction angle φ_{max} is calculated by way of $\sin\varphi_{max} = q_f/(q_f + 2\sigma_3)$, and q_f is the peak deviatoric stress. As shown in Fig. 8(a), the peak friction angle decreased with increasing confining pressure and overall

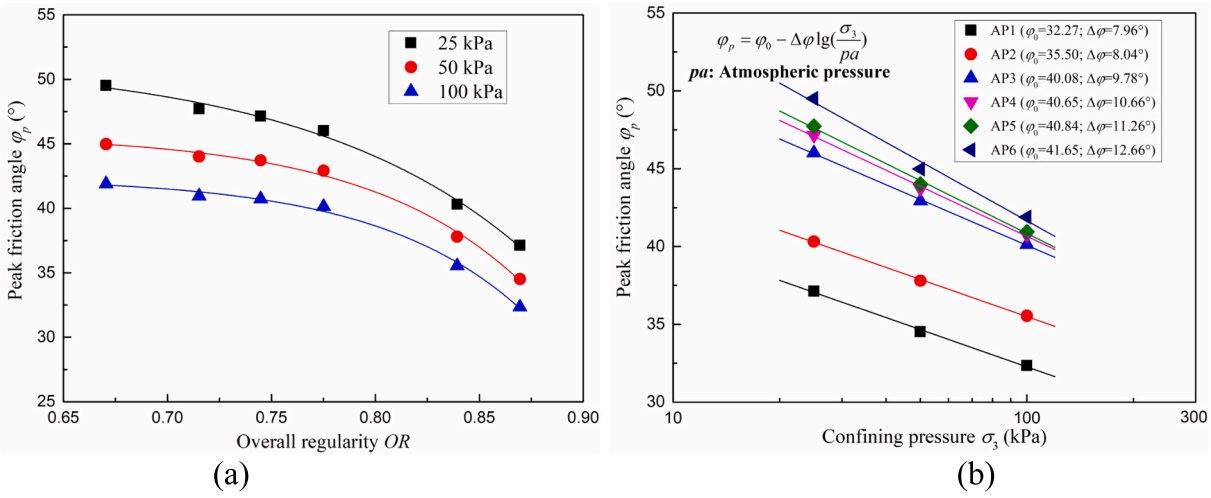

Fig. 8. Peak friction angles of the cereals after staining (a) relationship between φ_p and OR (b) relationship between φ_p and σ_3.

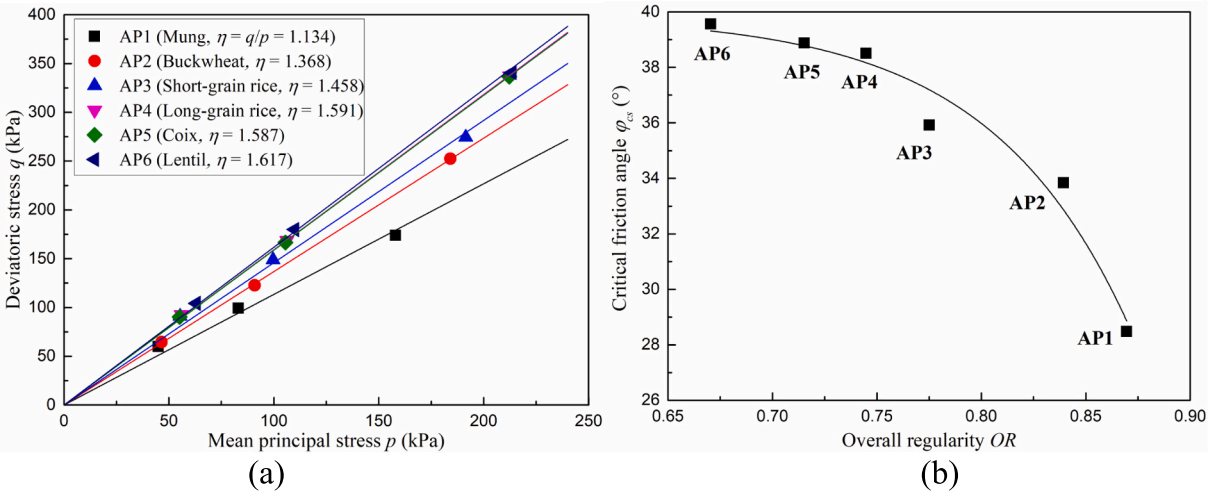

Fig. 9. Critical friction angles of the cereals after staining (a) relationship between q and p (b) relationship between φ_{cs} and OR.

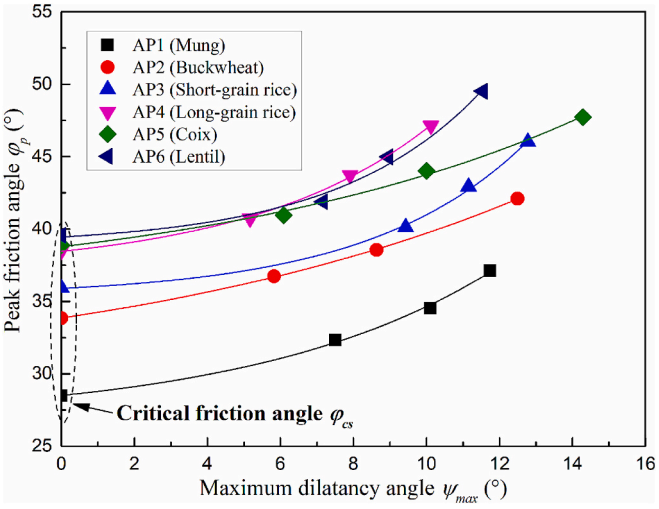

Fig. 10. Relationship between φ_p and ψ_{max} of the cereals after staining.

regularity. It indicated that the agricultural particle with more irregularity under smaller confining pressure had a larger peak friction angle, and the overall regularity could properly characterize the variation trend of the peak friction angle with particle shape. In addition, Fig. 8(b) shows the relationship between the peak friction angle φ_{max} and the confining pressure σ_3 for six types of cereals. pa is the atmospheric pressure. It can be found that the peak friction angle φ_{max} and the confining pressure σ_3 had an approximately linear relationship in semilogarithmic coordinates, and the slope $\Delta\varphi$ increased with increasing overall regularity OR.

Fig. 9(a) shows the relationship between deviatoric stress q ($=\sigma_1$-σ_3) and mean principal stress p [$=(\sigma_1 + 2\sigma_3)/3$] for six types of cereals at an axial strain of 25 %. It can be observed that for the same agricultural particle, the stress ratios η ($=q/p$) at different confining pressures approached the same value, and the friction angle at an axial strain of 25 % was approximately the critical state friction angle φ_{cs}. The stress ratios for the mung, buckwheat, short-grain rice, long-grain rice, coix and lentil were 1.134, 1.368, 1.458, 1.591, 1.587 and 1.617, respectively. Fig. 9(b) shows the relationship between the critical state friction angle φ_{cs} and the overall regularity OR. Similar to the peak friction angle, the critical state friction angle decreased with increasing overall regularity, indicating a larger critical state friction angle for irregular particles.

Fig. 10 shows the relationship between the peak friction angle $\varphi_{\max}$

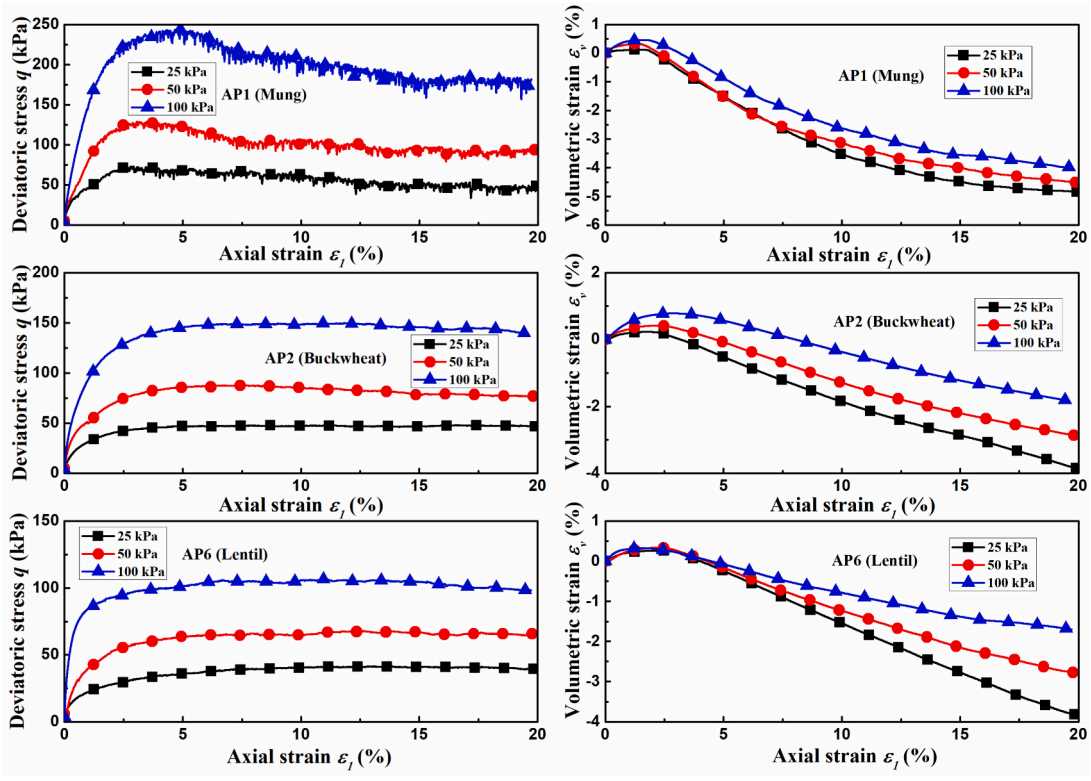

(a)

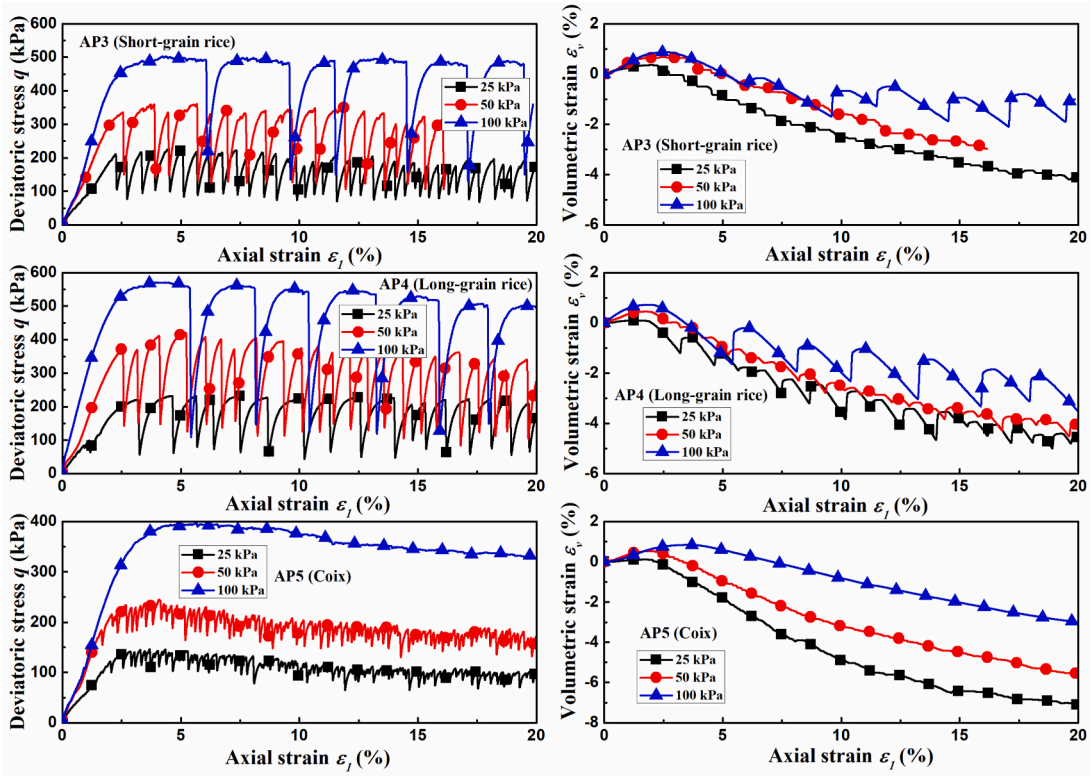

(b)

Fig. 11. Monotonic stress-strain relationships of the original cereals (a) with seed coat (b) without seed coat.

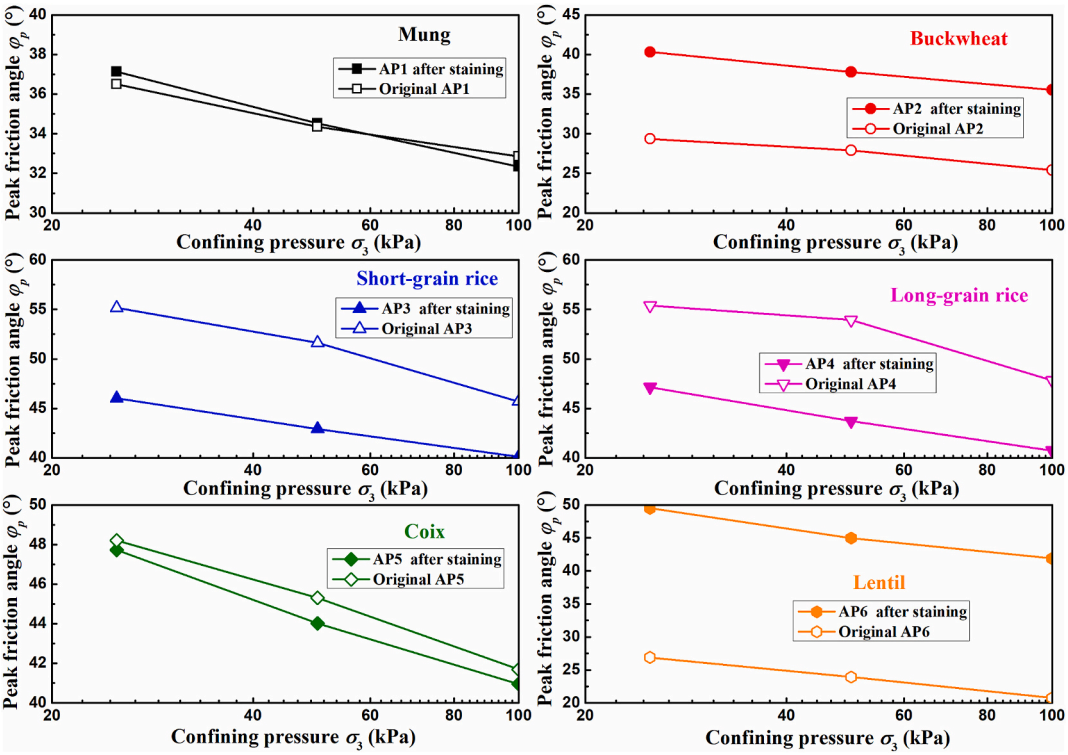

Fig. 12. Peak friction angle comparison for cereals before and after staining.

and the maximum dilatancy angle ψ_{max} for six types of cereals. The maximum dilation angle ψ_{max} is calculated by way of $\sin\psi_{max} = [d\varepsilon_v/(2d\varepsilon_1\text{-}d\varepsilon_v)]_{max}$. $d\varepsilon_v$ and $d\varepsilon_1$ are the volumetric strain and axial strain increments, respectively. It can be observed that a unique relationship existed between the peak friction angle and the maximum dilatancy angle for the same agricultural particle. However, different from the hard granular materials [13] (i.e. sand or glass bead), the φ_{max} - ψ_{max} curve for the soft cereals appeared to be a nonlinear curve rather than a straight line. Due to limited test data in this study, further investigation is required to obtain definite conclusions.

4.2. *Effect of surface characteristics*

The cereals can be divided into two types: particles with (i.e. mung, buckwheat and lentil) and without (i.e. short-grain rice, long-grain rice and coix) seed coat. Figs. 11(a) and (b) show monotonic deviatoric stress-volumetric strain-axial strain relationships of the original cereals with and without seed coat, respectively. As shown in Fig. 11, the seed coat had a significant effect on the monotonic stress-strain relationships of cereals. The peak deviatoric stresses of the cereals without seed coat were significantly larger than that of the cereals with seed coat. However, the cereals without seed coat (as shown in Fig. 11(b)), especially the short-grain and long-grain rice, experienced the phenomenon of abrupt loss of load-bearing capacity during monotonic shearing, which occurred more frequently at lower confining pressures. The abrupt strength loss of the specimen was also accompanied by the abrupt contraction of the specimen, as shown in Fig. 11(b). The possible reason was that the bond of surface starch on the cereals without seed coat formed under confining pressure, with the bond significantly enhancing their shear strength. However, the bond of surface starch was insufficiently stable, rupturing when deviatoric stress reached the critical threshold, resulting in abrupt strength loss. During subsequent loading, the load-bearing capacity of specimen recovered due to the formation of new bond under confining pressure. Furthermore, the phenomenon occurred less frequently at higher confining pressure due to the higher confining pressure making the bond more stable. The surface starch of coix was less than that of rice (as shown in SEM images in Fig. 1(a)), so its phenomenon was more insignificant and its peak stress was lower. For the cereals without seed coat after staining, the phenomenon disappeared because the acrylic paint prevented the bond of surface starch. In addition, it can be found from Fig.11(a) that the deviatoric stress-axial strain curves of mung were fluctuating, and the fluctuation was more significant at higher confining pressure. The phenomenon was also found in the glass beads [19,56] and donated as stick-slip behavior, which involved a transition from static to dynamic processes. When the deviatoric stress exceeded the threshold of particle interaction resisting sliding, noticeable sliding and rearrangement of the particles within the specimens occurred, leading to instantaneous fluctuations on the macroscale stress-strain curves [19,56]. However, the stick-slip behavior was not observed in buckwheat and lentil probably due to their irregular particle shape.

Fig. 12 shows the peak friction angle comparison for cereals before and after staining. Changes in the surface roughness of cereal particles before and after staining were determined by comparing their angles of repose. The angle of repose tests on cereals before and after staining showed that staining had no significant effect on the surface roughness of mung beans but significantly increased roughness for all other cereals (as shown in Figs. 5 and 6). For the cereals with seed coat (i.e. mung, buckwheat and lentil), the staining mainly changed their surface roughness, leading to a change in the inter-particle friction coefficient. It can be observed that the peak friction angles of mung remained basically unchanged after staining, while the peak friction angles of buckwheat and lentil increased significantly after staining, which was consistent with the change of their surface roughness after staining. This indicates that the shear strength of granular materials was highly related to the inter-particle friction coefficient, and the shear strength increased with increasing inter-particle friction coefficient.

However, for the cereals without seed coat (i.e. short-grain rice, long-grain rice and coix), although the staining significantly increased their surface roughness, their peak friction angle significantly decreased after staining due to the acrylic paint preventing the bond of surface starch.

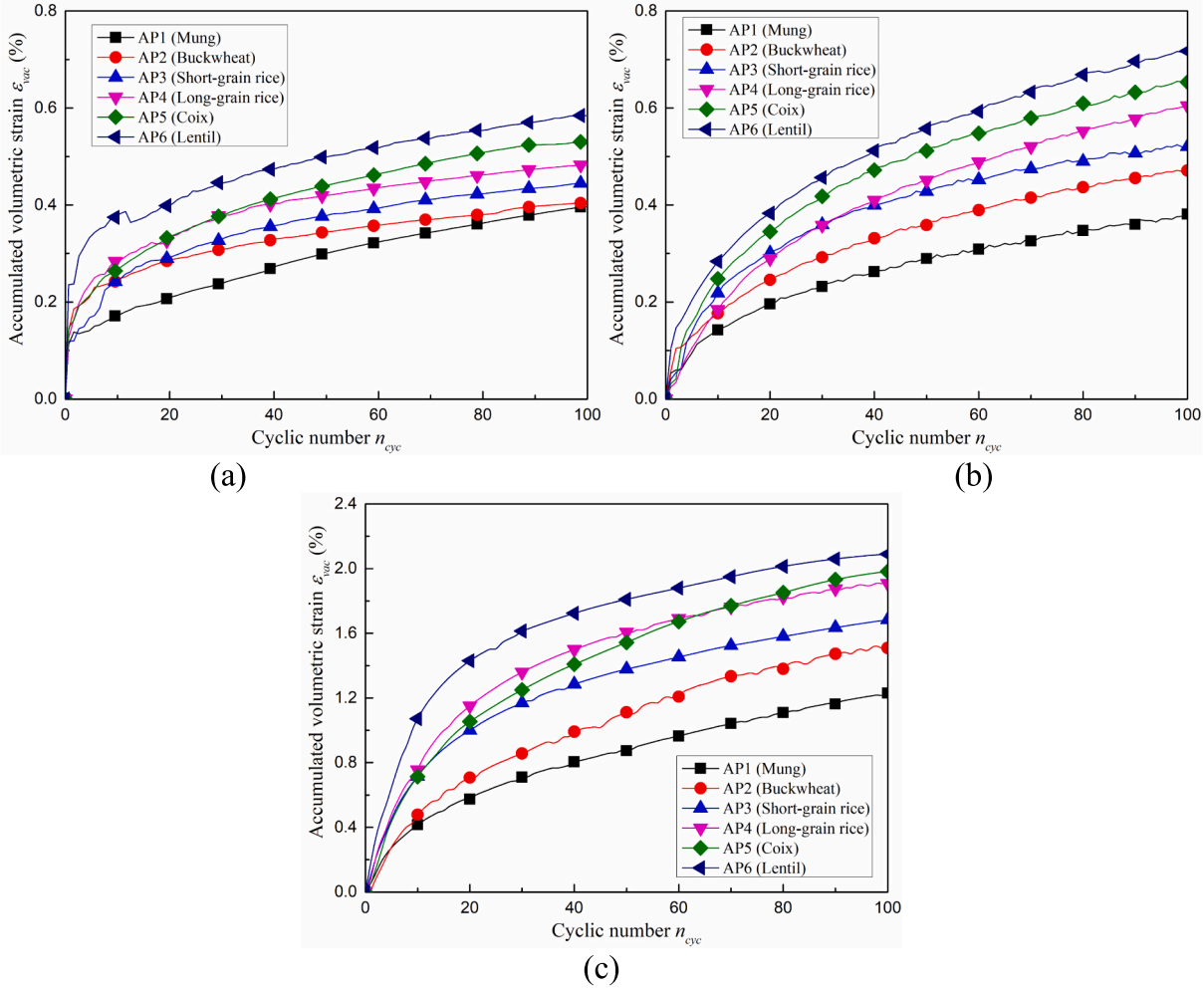

Fig. 13. Relationship between ε_{vac} and n_{cyc} of the cereals after staining (a) one-way stress cyclic tests (b) two-way stress cyclic tests (c) strain cyclic tests.

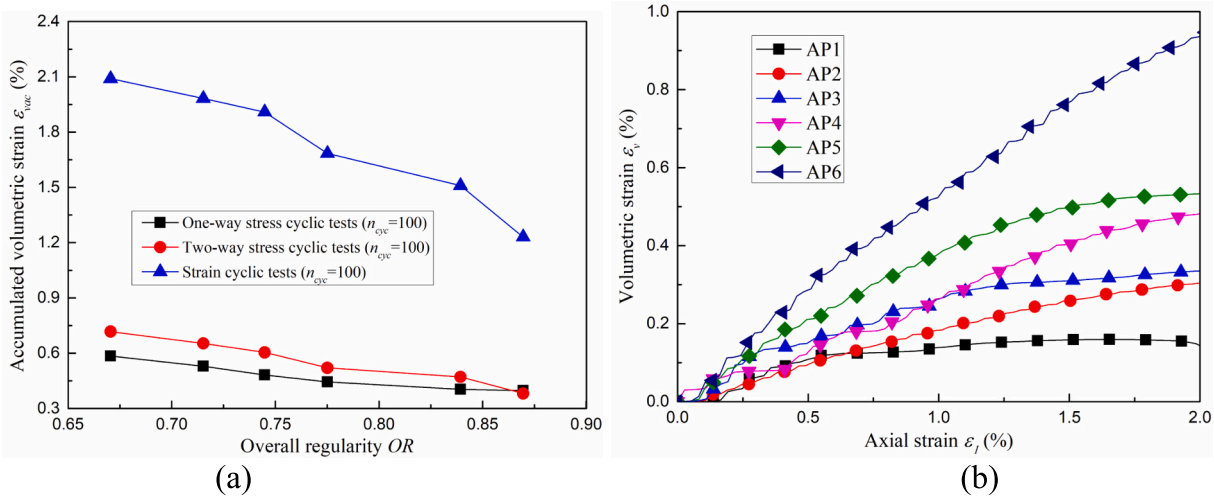

Fig. 14. Effect of overall regularity on the volumetric strain (a) Relationship between ε_{vac} and OR of the cereals after staining (b) monotonic volumetric strain-axial strain curves at 0 %–2 % axial strain range.

5. Cyclic mechanical behavior

In this section, the analyses focused on the variation of accumulated volumetric strains during cyclic triaxial tests. Considering space restriction, the cyclic deviatoric stress-volumetric strain-axial strain curves of six types of cereals are placed in Figs. S1-S6 of the Supplemental Materials. Notably, the phenomenon of abrupt bearing capacity loss was not observed in the cyclic tests because the deviatoric stress level was far below the peak value.

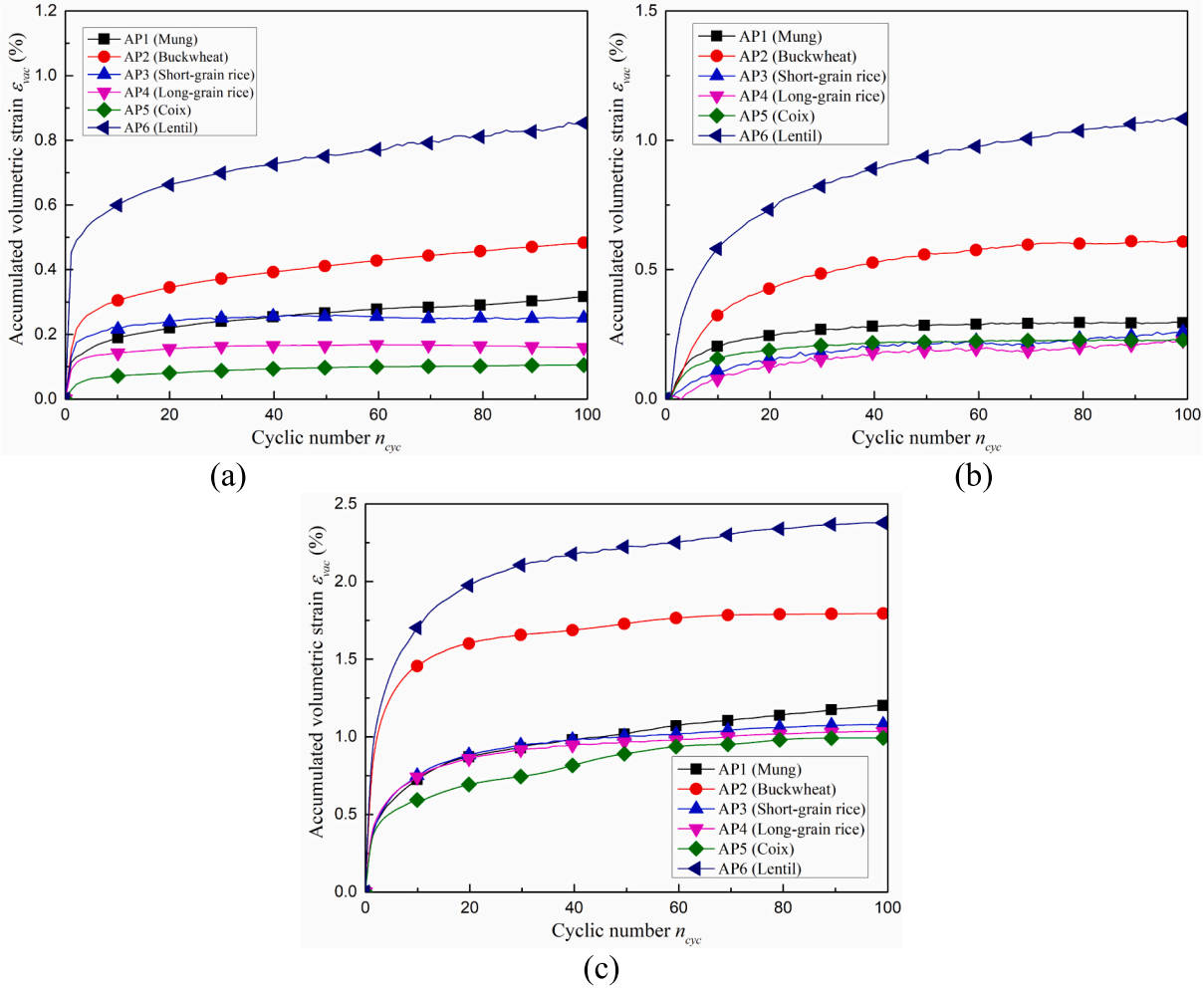

Fig. 15. Relationship between ε_{vac} and n_{cyc} of the original cereals (a) one-way stress cyclic tests (b) two-way stress cyclic tests (c) strain cyclic tests.

5.1. *Effect of particle shape*

Fig. 13 shows the relationship between the accumulated volumetric strain ε_{vac} and the cyclic number n_{cyc} of the stained cereals in three cyclic triaxial tests. It can be found that the accumulated volumetric strain exhibited an approximate hyperbolic relationship with the cyclic number under all three cyclic loading methods. The accumulated volumetric strain increased with increasing cyclic number, but the increasing rate gradually decreased. In addition, it can be found by comparing the results of mung particles with other cereals that the accumulated volumetric strain at the same cyclic number decreased with increasing elongation *EI*, flatness *FI*, sphericity *S*, convexity *C* and

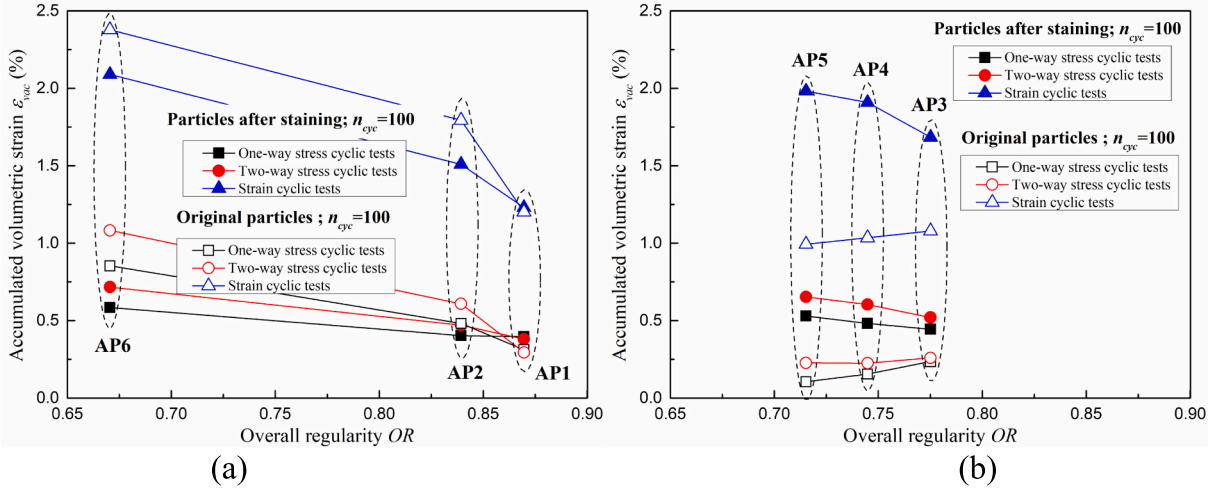

Fig. 16. Accumulated volumetric strain comparison for cereals before and after staining (a) with seed coat (b) without seed coat.

roundness *R*.

Fig. 14(a) shows the relationship between the accumulated volumetric strain at 100 cycles and the overall regularity *OR* under different cyclic loading methods. It can be seen that for the same agricultural particle, the accumulated volumetric strain in the strain cyclic tests was the largest, followed by the two-way stress cyclic tests, and the accumulated volumetric strain was the smallest in the one-way stress cyclic tests. Furthermore, the accumulated volumetric strain at 100 cycles decreased with increasing overall regularity. The cyclic axial strains for all three cyclic triaxial tests were in the range of 0 % to 2 %, and the monotonic volumetric strain-axial strain curves for six types of cereals near this range are also shown in Fig. 14(b). It can be observed that similar to the accumulated volumetric strain, the maximum volumetric strain of cereals during monotonic loading also decreased with increasing overall regularity. This indicated that the agricultural particle with more irregularity had a larger compressibility when the axial strain was small.

5.2. Effect of surface characteristics

Fig. 15 shows the relationship between the accumulated volumetric strain ε_{vac} and the cyclic number n_{cyc} of the original cereals in three cyclic triaxial tests. It can be found that the accumulated volumetric strain of the original cereals also exhibited an approximate hyperbolic relationship with the cyclic number. However, due to the combined effect of surface characteristics and particle shape, the ranking of accumulated volumetric strain for the original cereals was significantly different from that for the stained cereals.

Fig. 16 shows the accumulated volumetric strain comparison for cereals before and after staining. It can be found that for the cereals with seed coat (i.e. AP1 mung, AP2 buckwheat and AP6 lentil), the accumulated volumetric strains of mung remained basically unchanged after staining, while the accumulated volumetric strains of buckwheat and lentil decreased after staining. It indicated that the granular materials with larger friction coefficient might be more difficult to be compressed during cyclic loading. For the cereals without seed coat (i.e. AP3 short-grain rice, AP4 long-grain rice and AP5 coix), the deviatoric stress level during cyclic loading was low and did not reach the critical threshold of starch bond rupture, and the bond greatly increased the stability of the granular system, resulting in a significantly lower compressibility of the unstained specimens.

6. Conclusions

In this study, six types of cereals before and after staining were selected for a series of monotonic and cyclic triaxial tests. The effect of particle shape and surface characteristics on their mechanical behavior was analyzed. The major findings are summarized below.

(1) The overall regularity *OR* was used to characterize the comprehensive shape of cereals in this study, and the test results showed that the peak and critical friction angles of cereals decreased with increasing overall regularity *OR*. In addition, different from the hard granular materials, the relationship between the peak friction angle and the maximum dilatancy angle for the soft cereals were a concave up curve rather than a straight line.
(2) The cyclic triaxial test results showed that for the same agricultural particle, the accumulated volumetric strain in the strain cyclic tests was the largest, followed by the two-way stress cyclic tests, and the accumulated volumetric strain was the smallest in the one-way stress cyclic tests. Furthermore, the accumulated volumetric strain of cereals decreased with increasing overall regularity *OR*.
(3) It can be found by comparing the test results of the cereals with seed coat before and after staining that the particles with rougher surface had a larger peak friction angle and were more difficult to be compressed during cyclic loading.
(4) For the cereals without seed coat, their surface starch would bond under confining pressure, resulting in a significantly larger peak friction angle and a lower compressibility of the specimen during cyclic loading. However, when the deviatoric stress reached the critical threshold of starch bond rupture, the specimens experienced an abrupt strength reduction and volume contraction. This phenomenon requires special attention during the storage and transportation of cereals. Furthermore, due to the acrylic paint preventing the bond of surface starch, the peak friction angle and the accumulated volumetric strain of the cereals without seed coat significantly decreased after staining.

This study comprehensively investigated the effects of particle morphology and surface characteristics on the monotonic and cyclic mechanical behavior of granular materials through laboratory experiments. Some valuable findings were obtained. However, it is worth noting that the conclusions of this study are based on specimens with identical relative density. Distinct findings might emerge if experiments were conducted under the same void ratios. The effects of particle morphology and surface characteristics on the behavior of granular materials warrant further study.

CRediT authorship contribution statement

Kaifeng Zeng: Writing – original draft, Visualization, Methodology. **Zhen-Yu Yin**: Funding acquisition, Writing – review & editing, Supervision. **Ruidong Li**: Visualization. **Yin-Fu Jin**: Supervision.

Declaration of competing interest

The authors declare that they have no known competing financial interests or personal relationships that could have appeared to influence the work reported in this paper.

Acknowledgment

This work was supported by the general research fund of the Research Grants Council (RGC) of the Hong Kong Special Administrative Region Government (HKSARG) of China (grant No. 15229223, 15227923, 15226322, 15220221).

Appendix A. Supplementary data

Supplementary data to this article can be found online at https://doi.org/10.1016/j.powtec.2025.121452.

Data availability

Data will be made available on request.

References

[1] Y. Cui, Y. Li, H. Tang, J.M. Turowski, Y. Yan, N.A. Bazai, R. Wei, L. Li, A digital-twin platform for cryospheric disaster warning, Natl. Sci. Rev. 11 (10) (2024), https://doi.org/10.1093/nsr/nwae300 nwae300.
[2] X. Zhou, Y. Cui, J. Fang, H. Tang, Z. Zhang, S. Wang, Link between the impact mechanisms of granular flow-dam interaction and the generated seismic signal: Insights from laboratory experiments, J. Geophys. Res. Solid Earth 130 (4) (2025), https://doi.org/10.1029/2024JB029946 e2024JB029946.
[3] J.Y. Nie, Y. Cui, G. Wang, R. Wang, N. Zhang, L. Zhang, Z. Wu, A comprehensive numerical investigation of multi-scale particle shape effects on small-strain stiffness of sands, Géotechnique 75 (3) (2024) 323–336, https://doi.org/10.1680/jgeot.23.00118.
[4] J. Nie, S. Zhao, Y. Cui, Y. Wang, Coupled effects of particle overall regularity and sliding friction on the shear behavior of uniformly graded dense sands, J. Rock Mech. Geotech. Eng. 14 (3) (2022) 873–885, https://doi.org/10.1016/j.jrmge.2021.10.014.

[5] G.C. Cho, J. Dodds, J.C. Santamarina, Particle shape effects on packing density, stiffness, and strength: natural and crushed sands, J. Geotech. Geoenviron. Eng. 132 (5) (2006) 591–602, https://doi.org/10.1061/(ASCE)1090-0241(2006)132:5(591).

[6] H. Shin, J.C. Santamarina, Role of particle angularity on the mechanical behavior of granular mixtures, J. Geotech. Geoenviron. Eng. 139 (2) (2013) 353–355, https://doi.org/10.1061/(asce)gt.1943-5606.0000768.

[7] R. Rorato, M. Arroyo Alvarez de Toledo, E.C.G. Ando, A. Gens, G. Viggiani, Linking shape and rotation of grains during triaxial compression of sand, Granul, Matter 22 (4) (2020) 1–21, https://doi.org/10.1007/s10035-020-01058-2.

[8] S.S. Ahmed, A. Martinez, Triaxial compression behavior of 3D printed and natural sands, Granul. Matter 23 (4) (2021) 82, https://doi.org/10.1007/s10035-021-01143-0.

[9] U. Ali, M. Kikumoto, Experimental micro-macromechanics: critical states of round/angular granular mixtures, J. Geotech. Geoenviron. Eng. 150 (12) (2024) 04024129, https://doi.org/10.1061/JGGEFK.GTENG-12582.

[10] R. Qu, C.H. Ma, C.Q. Zhu, H.F. Liu, Experimental study on the influence of particle morphology on compression characteristics of coral sand in South China Sea, Ocean Eng. 312 (2024) 119339, https://doi.org/10.1016/j.oceaneng.2024.119339.

[11] K. Shinohara, M. Oida, B. Golman, Effect of particle shape on angle of internal friction by triaxial compression test, Powder Technol. 107 (1–2) (2000) 131–136, https://doi.org/10.1016/S0032-5910(99)00179-5.

[12] F.N. Altuhafi, M.R. Coop, V.N. Georgiannou, Effect of particle shape on the mechanical behavior of natural sands, J. Geotech. Geoenviron. Eng. 142 (12) (2016) 04016071, https://doi.org/10.1061/(ASCE)GT.1943-5606.0001569.

[13] Y. Xiao, L. Long, T. Matthew Evans, H. Zhou, H. Liu, A.W. Stuedlein, Effect of particle shape on stress-dilatancy responses of medium-dense sands, J. Geotech. Geoenviron. Eng. 145 (2) (2019) 04018105, https://doi.org/10.1061/(asce)gt.1943-5606.0001994.

[14] M. Haruyama, Effect of surface roughness on the shear characteristics of granular materials, Soils Found. 9 (4) (1969) 48–67, https://doi.org/10.3208/sandf1960.9.4_48.

[15] M. Otsubo, C. O'Sullivan, K.J. Hanley, W.W. Sim, The influence of particle surface roughness on elastic stiffness and dynamic response, Géotechnique 67 (5) (2017) 452–459, https://doi.org/10.1680/jgeot.16.P.050.

[16] X. Li, M. Dong, D. Jiang, S. Li, Y. Shang, The effect of surface roughness on normal restitution coefficient, adhesion force and friction coefficient of the particle-wall collision, Powder Technol. 362 (2020) 17–25, https://doi.org/10.1016/j.powtec.2019.11.120.

[17] V. Marzulli, C.S. Sandeep, K. Senetakis, F. Cafaro, T. Pöschel, Scale and water effects on the friction angles of two granular soils with different roughness, Powder Technol. 377 (2021) 813–826, https://doi.org/10.1016/j.powtec.2020.09.060.

[18] Y. Li, M. Otsubo, J. Liu, R. Kuwano, Effect of particle morphology on stress and strain characteristics of granular materials during triaxial compression, Acta Geotech. 19 (5) (2024) 2753–2773, https://doi.org/10.1007/s11440-023-02190-y.

[19] M. Miao, F. Liu, Y. Yin, Y. Tang, L. Zhong, The influence of surface roughness on the shear mechanical behavior of 2 mm spherical particle materials, Granul. Matter 27 (1) (2025) 1–14, https://doi.org/10.1007/s10035-024-01497-1.

[20] U. Ali, M. Kikumoto, M. Ciantia, Y. Cui, M. Previtali, Systematic effect of particle roundness/angularity on macro- and microscopic behavior of granular materials, Granul. Matter 25 (3) (2023) 51, https://doi.org/10.1007/s10035-023-01341-y.

[21] H.B.K. Nguyen, M.M. Rahman, A.B. Fourie, How particle shape affects the critical state, triggering of instability and dilatancy of granular materials – results from a DEM study, G'eotechnique 74 (12) (2020) 1503–1508, https://doi.org/10.1680/jgeot.18.p.211.

[22] J.M. Ting, L. Meachum, J.D. Rowell, "Effect of particle shape on the strength" and deformation mechanisms of ellipse—shaped granular assemblages, Eng. Comput. 12 (2) (1995) 99–108, https://doi.org/10.1108/02644409510799497.

[23] A.A. Mirghasemi, L. Rothenburg, E.L. Matyas, Influence of particle shape on engineering properties of assemblies of two-dimensional polygon-shaped particles, Geotechnique 52 (3) (2002) 209–217, https://doi.org/10.1680/geot.2002.52.3.209.

[24] Z. Nie, S. Liu, W. Hu, J. Gong, Effect of local non-convexity on the critical shear strength of granular materials determined via the discrete element method, Particuology 52 (2021) (2020) 105–112, https://doi.org/10.1016/j.partic.2019.12.008.

[25] S. Zhao, X. Zhou, W. Liu, Discrete element simulations of direct shear tests with particle angularity effect, Granul. Matter 17 (6) (2015) 793–806, https://doi.org/10.1007/s10035-015-0593-x.

[26] M. Wu, L. Xiong, J. Wang, DEM study on effect of particle roundness on biaxial shearing of sand, Undergr. Sp. 6 (6) (2021) 678–694, https://doi.org/10.1016/j.undsp.2021.03.006.

[27] J. Gong, J. Liu, Effect of aspect ratio on triaxial compression of multi-sphere ellipsoid assemblies simulated using a discrete element method, Particuology 32 (2017) 49–62, https://doi.org/10.1016/j.partic.2016.07.007.

[28] Y.H. Xie, Z.X. Yang, D. Barreto, M.D. Jiang, The influence of particle geometry and the intermediate stress ratio on the shear behavior of granular materials, Granul. Matter 19 (2) (2017) 1–13, https://doi.org/10.1007/s10035-017-0723-8.

[29] C.M. Wensrich, A. Katterfeld, D. Sugo, Characterisation of the effects of particle shape using a normalised contact eccentricity, Granul. Matter 16 (3) (2014) 327–337, https://doi.org/10.1007/s10035-013-0465-1.

[30] J.Y. Nie, J. Zhao, Y.F. Cui, D.Q. Li, Correlation between grain shape and critical state characteristics of uniformly graded sands: a 3D DEM study, Acta Geotech. 17 (2022) 2783–2798, https://doi.org/10.1007/s11440-021-01362-y.

[31] X. Liu, K. Zeng, F. Xiang, C. Wang, X. Hou, Y. Li, Study on the interaction between particle shape and particle breakage of coral sand by discrete element method, Front. Earth Sci. 12 (2024) 1343307, https://doi.org/10.3389/feart.2024.1343307.

[32] J. Kozicki, J. Tejchman, Z. Mróz, Effect of grain roughness on strength, volume changes, elastic and dissipated energies during quasi-static homogeneous triaxial compression using DEM, Granul. Matter 14 (2012) 457–468, https://doi.org/10.1007/s10035-012-0352-1.

[33] M.M. Thakur, D. Penumadu, Influence of friction and particle morphology on triaxial shearing of granular materials, J. Geotech. Geoenviron. Eng. 147 (11) (2021) 04021118, https://doi.org/10.1061/(ASCE)GT.1943-5606.0002634.

[34] M.Q. Xu, N. Guo, Z.X. Yang, Particle shape effects on the shear behaviors of granular assemblies: irregularity and elongation, Granul. Matter 23 (2021) 25, https://doi.org/10.1007/s10035-021-01096-4.

[35] Z. Nie, C. Fang, J. Gong, Z. Liang, DEM study on the effect of roundness on the shear behaviour of granular materials, Comput. Geotech. 121 (2020) 103457, https://doi.org/10.1016/j.compgeo.2020.103457.

[36] U. Ali, M. Kikumoto, Role of particle shape in sheared granular media: roundness and elongation, Powder Technol. 449 (2025) 120436, https://doi.org/10.1016/j.powtec.2024.120436.

[37] M. Fan, D. Su, X. Chen, Systematic investigation into the role of particle multi-level morphology in determining the shear behavior of granular materials via DEM simulation, Comput. Geotech. 170 (2024) 106298, https://doi.org/10.1016/j.compgeo.2024.106298.

[38] C. Zeng, X. Li, Y. Wang, Behaviour of the interface between stored wheat and a steel silo under static and cyclic loading conditions, Biosyst. Eng. 190 (2020) 87–96, https://doi.org/10.1016/j.biosystemseng.2019.11.024.

[39] G. Pinzón, E. Andò, J. Desrues, G. Viggiani, Fabric evolution and strain localisation in inherently anisotropic specimens of anisometric particles (lentils) under triaxial compression, Granul. Matter 25 (1) (2023) 15, https://doi.org/10.1007/s10035-022-01305-8.

[40] M.C. Petingco, M.E. Casada, R.G. Maghirang, O.O. Fasina, Z. Chen, R.K. Ambrose, Influence of particle shape and contact parameters on DEM-simulated bulk density of wheat, Trans. ASABE 63 (6) (2020) 1657–1672, https://doi.org/10.13031/trans.13718.

[41] M. Molenda, M.D. Montross, J. Horabik, I.J. Ross, Mechanical properties of corn and soybean meal, Transactions of the ASAE 45 (6) (2002) 1929–1936, https://doi.org/10.13031/2013.11408.

[42] M. Moya, F. Ayuga, M. Guaita, P. Aguado, Mechanical properties of granular agricultural materials, Transactions of the ASAE 45 (5) (2002) 1569, https://doi.org/10.13031/2013.11062.

[43] M. Moya, P.J. Aguado, F. Ayuga, Mechanical properties of some granular agricultural materials used in silo design, International Agrophysics 27 (2) (2013) 181–193, https://doi.org/10.2478/v10247-012-0084-9.

[44] S. Singh, B.A. Baudet, M.R. Coop, Particulate behaviour of soft granular materials: a case study on lentils, Granul. Matter 27 (1) (2025) 1–17, https://doi.org/10.1007/s10035-025-01506-x.

[45] H. Kibar, T. Ozturk, Physical and mechanical properties of soybean, Int. Agrophys. 22 (3) (2008) 239–244, https://doi.org/10.1002/pssa.200306757.

[46] ASTM. Standard test methods for maximum index density and unit weight of soils using a vibratory table, ASTM D4253-16, West Conshohocken, ASTM, PA, 2016.

[47] R. Li, P. Zhang, Z.Y. Yin, B. Sheil, Enhanced hybrid algorithms for segmentation and reconstruction of granular grains from X-ray micro computed-tomography images, Int. J. Numer. Anal. Methods Geomech. 48 (17) (2024) 4206–4220, https://doi.org/10.1002/nag.3832.

[48] R.D. Li, Z.Y. Yin, S.H. He, 3D reconstruction of arbitrary granular media utilizing vision foundation model, Appl. Soft Comput. 169 (2025) 112599, https://doi.org/10.1016/j.asoc.2024.112599.

[49] R. Li, Z.Y. Yin, S. He, B. Sheil, Enhancement and assessment of large vision models for 3D particle reconstruction from X-ray tomography, Can. Geotech. J. 62 (2025) 1–28, https://doi.org/10.1139/cgj-2024-0736.

[50] E.D. Sneed, R.L. Folk, Pebbles in the lower Colorado River, Texas a study in particle morphogenesis, J. Geol. 66 (2) (1958) 114–150, https://doi.org/10.1086/626490.

[51] S.J. Blott, K. Pye, Particle shape: a review and new methods of characterization and classification, Sedimentology 55 (1) (2008) 31–63, https://doi.org/10.1111/j.1365-3091.2007.00892.x.

[52] H. Wadell, Volume, shape, and roundness of rock particles, J. Geol. 40 (5) (1932) 443–451, https://doi.org/10.1086/623964.

[53] ASTM. Standard test method for consolidated drained triaxial compression test for soils, ASTM D7181., West Conshohocken, ASTM, PA, 2011.

[54] K. Zeng, H. Liu, Effect of inherent anisotropy on the triaxial compression behavior of coral sand, Int. J. Geomech. 23 (5) (2023) 04023033, https://doi.org/10.1061/IJGNAI.GMENG-8003.

[55] H. Liu, K. Zeng, Y. Zou, Particle breakage of calcareous sand and its correlation with input energy, Int. J. Geomech. 20 (2) (2020) 04019151, https://doi.org/10.1061/(ASCE)GM.1943-5622.0001541.

[56] D. Cui, W. Wu, W. Xiang, T. Doanh, Q. Chen, S. Wang, Q. Liu, J. Wang, Stick-slip behaviours of dry glass beads in triaxial compression, Granul. Matter 19 (2017) 1–18, https://doi.org/10.1007/s1 0035–016–0682-5.